Further Analysis of Wing Rock Generated by Forebody Vortices

L. E. Ericsson*
Lockheed Missiles & Space Company, Inc., Sunnyvale, California

Further analysis of wing rock generated by forebody vortices has revealed a richness of flow phenomena that can produce the rather violent forms of wing-body rock observed experimentally. Relatively mild changes of the aircraft geometry cause different flow mechanisms to become the dominant ones, dictating the nature of the wing rock. The general observation is that the wing rock generated by vortices from a slender forebody not only is much more severe than slender wing rock, generated by asymmetric, leading-edge vortices, but it is also the type of wing rock to which most current and future advanced aircraft will be exposed.

Nomenclature

b = wing span
c_r = wing root chord
d = diameter of cylindrical aft body
l_N = length of pointed, ogival nose
ℓ = sectional lift, coefficient $c_\ell = \ell/(\rho_\infty U_\infty{}^2/2)d$
$\acute{\ell}$ = rolling moment, coefficient $C_\ell = \acute{\ell}/(\rho_\infty U_\infty{}^2/2)Sb$
p = body spin rate
Re = Reynolds number, $Re = U_\infty d/\nu_\infty$
S = wing area
t = time
Δt = time lag
U = velocity
$\bar{U}$ = mean convection velocity
x = axial distance from apex
Y = side force, coefficient $C_y = Y/(\rho_\infty U_\infty{}^2/2)\ \pi d^2/4$
Λ = leading edge sweep angle
Δ = amplitude and increment
α = angle of attack
α_0 = trim angle of attack
θ_A = apex half angle
ν = kinematic viscosity
ρ = air density
σ = inclination of cross-flow plane (Fig. 11)
ϕ = roll angle

Subscripts

eff = effective
s = separation
W = wall
WR = wing rock
∞ = freestream conditions

Derivative Symbol

$\dot{\phi}$ = $\partial\phi/\partial t$

Introduction

THE violent wing rock exhibited by a generic fighter configuration in a subscale wind tunnel test[1] (see Fig. 1) was shown in Ref. 2 to be caused by so-called moving wall effects on boundary-layer transition in the forebody crossflow. The experimental results presented in Ref. 3 show the wing position (see Fig. 2) to have a pronounced effect on the wing-rock behavior (see Fig. 3). In the present paper, the flow concepts introduced in Ref. 2 are developed further and applied in an analysis aimed at finding the fluid mechanical reasons for the large effect on wing-rock characteristics of both wing position and forebody cross-sectional shape (see Fig. 3).

Discussion

According to the analysis in Ref. 2, the reason for the large amplitude wing rock for the model with a circular cross-sectional nose was that critical-flow conditions existed on the ogive-cylinder forebody. Moving the wing forward, close to the region where the vortices were generated for the aft wing position, eliminates that region as a source of forebody vortex shedding. In order to establish a wing-rock-generating flow mechanism similar to that occurring for the aft wing position, critical-flow conditions must be established on the circular cross-sectional nose well forward of the wing leading edge. Without increasing the test Reynolds number, this cannot happen. That explains the absence of wing rock at 30 deg $\leq \alpha < 40$ deg, the α region in which the maximum wing-rock amplitude was measured for the aft-wing position (compare Figs.

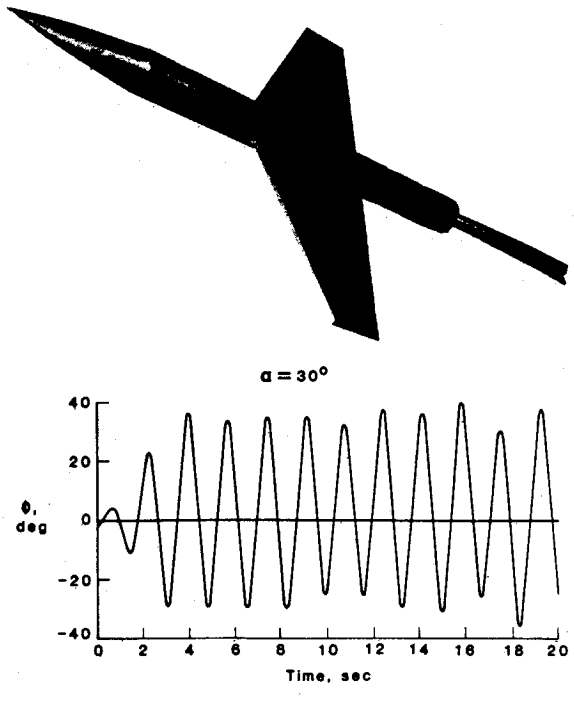

Fig. 1 Wing rock buildup at ∞ = 30 deg (Ref. 1).

Presented as Paper 88-2597 at the AIAA 6th Applied Aerodynamics Conference, Williamsburg, VA, June 6-8, 1988; received Dec. 12, 1988; revision received May 26, 1989.

*Senior Consulting Engineer. Fellow AIAA.

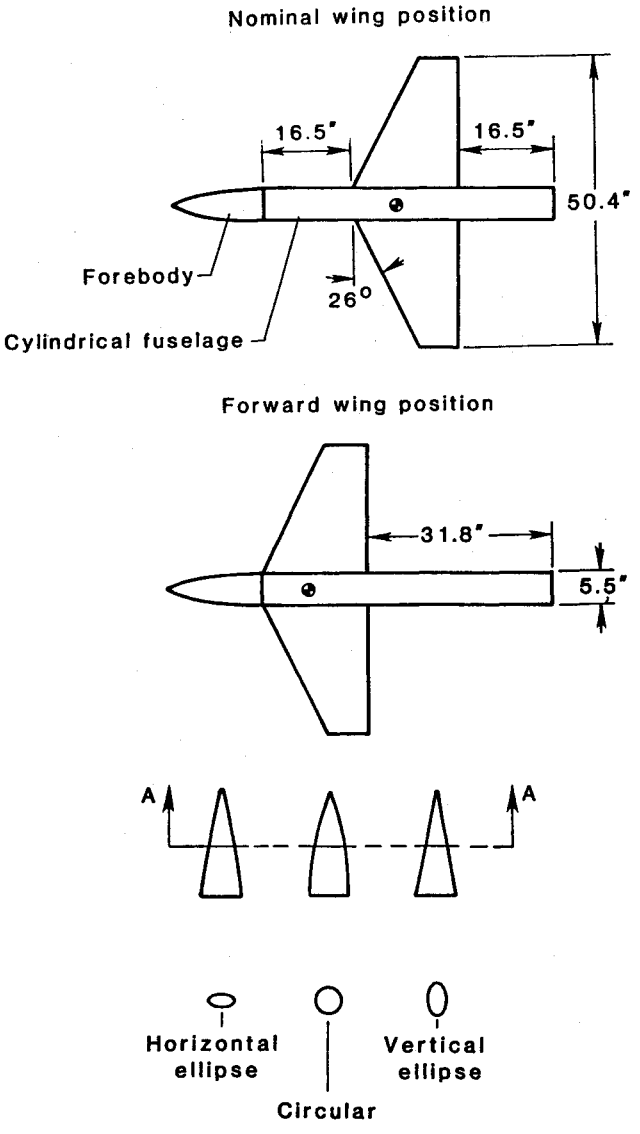

Fig. 2 Tested model geometries (Ref. 3).

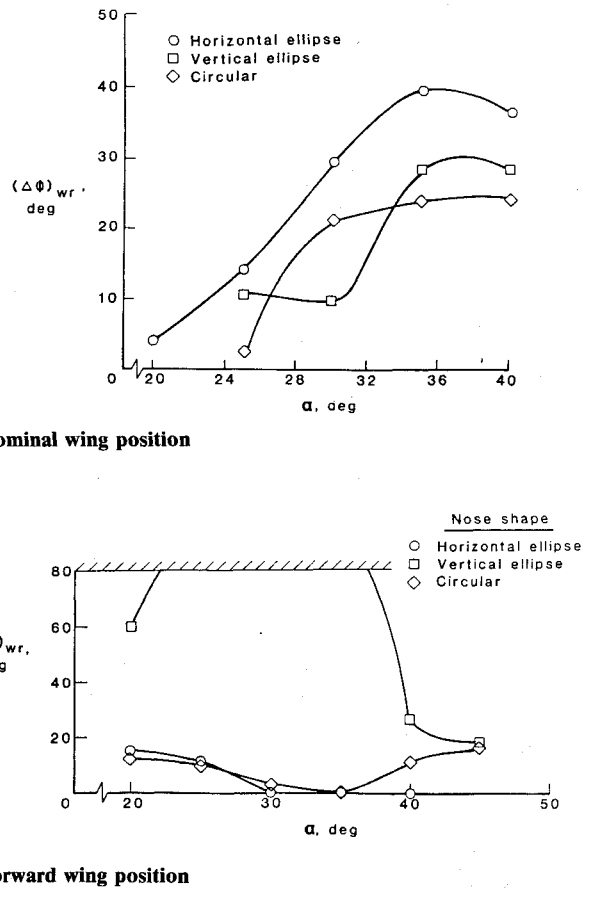

Fig. 3 Effect of nose cross-sectional geometry on wing-rock amplitude (Ref. 3).

3a and 3b). But what is the reason for the recurrence of wing rock at $\alpha < 30$ deg and $\alpha \geq 40$ deg and for the large effect of cross-sectional shape?

Analysis

In order to describe the coupling between vehicle motion and the flow phenomena of transition and flow separation, producing the wing-rock characteristics shown in Fig. 3, some recapitulation of the fluid mechanics behind the so-called moving wall effect[4] is needed.

Moving-Wall Effects

The classic Magnus lift of a rotating circular cylinder represents a well established case of moving-wall effects, and the experimental results presented by Swanson[5] will be used as a reference when discussing other types of moving-wall effects.

In the laminar case, where the separation at $p=0$ is of the subcritical type, the Magnus lift is generated mainly by the downstream moving wall effect on the top side, moving the separation from the subcritical toward the supercritical position (see Fig. 4). On the bottom side, the separation is already of the subcritical type at $p=0$, and the upstream moving-wall effect does not have much leverage for its separation-promoting action.

In the turbulent case (see Fig. 5), however, where the separation at $p=0$ is of the supercritical type, the situation is reversed. The main effect is that of the upstream moving wall on the bottom side, promoting separation, moving it from the supercritical toward the subcritical position. The difference in Magnus lift slopes, the turbulent one being three times as large as the laminar one, reflects the fact that the adverse (upstream) moving-wall effect is the largest, as would be expected.

These moving-wall effects are rather straightforward and explain the positive Magnus lift slopes. The negative slopes, the so-called Magnus lift reversals, are caused by the moving-wall effect on boundary-layer transition.[4] In the laminar case (see Fig. 4), when $p > p_{crit}$, the upstream moving-wall effect on the bottom side causes transition to occur before separation, changing the separation from the subcritical toward the supercritical type. This effect completely overpowers the regular moving-wall effects and causes a more or less discontinuous loss of lift (see Fig. 4). In the turbulent case (see Fig. 5), it is the downstream moving-wall effect on the top side that delays transition, causing it to move downstream of the separation point, and thereby changing the separation from the supercritical toward the subcritical type. This also generates a more or less discontinuous loss of lift.

In the Magnus lift reversals just discussed, the changes were towards, but not all the way to, the subcritical or supercritical types, the full change being restricted by the "regular" moving-wall effects. However, at critical-flow conditions, this restriction is no longer present. As a result, the lift loss is larger, and is generated immediately when p changes from $p=0$ to $p>0$ (see Fig. 6).

In the critical Reynolds number region, the flow separation is dominated by the presence of a laminar separation bubble (see Fig. 7). The boundary-layer turbulence generated by the

upstream moving-wall effect causes a forward movement of transition in the lifted shear layer forming the laminar separation bubble. As is sketched in Fig. 7b, the resulting separation delay produces increased suction, generating most of the measured negative Magnus lift shown in Fig. 6. A comparatively smaller contribution to the negative Magnus lift is generated by the transition delay caused by the downstream moving-wall effect on the opposite side, which promotes separation and causes a loss of suction.

The results shown in Figs. 4–7 are going to be used in what follows to explain the observed moving-wall effects for other body motions and other body geometries. It is shown in Refs. 4 and 6 that these two-dimensional moving-wall effects apply to bodies of revolution at $\alpha \geq 30$ deg.

Wing-Rock Characteristics

Comparing the wing-rock characteristics in Fig. 1 with those for an 80 deg sharp-edged delta wing[7] (see Fig. 8), one finds that the wing-body geometry in Fig. 1 reaches the 35 deg wing-rock amplitude in less than 3 cycles compared to 10 or more for the slender delta wing. Expanding somewhat on the flow concepts presented in Ref. 2, one can explain this difference in wing-rock characteristics as follows.

For the $l_N/d = 3$ tangent-ogive nose with circular cross section (Fig. 3a), the apex half angle is $\theta_A = 19$ deg. As one can safely assume the wing-induced upwash at apex to be negligible for the aft wing position, one does not expect symmetric forebody vortices to be generated until $\alpha > 19$ deg, and asymmetric vortices to appear only when $\alpha > 38$ deg.[6] Thus, the wing-rock amplitudes shown in Fig. 3a occurred on a configuration with initially symmetric vortices. As was discussed in Ref. 2, for the test Reynolds number,[1] $Re = 0.262 \times 10^6$, the critical conditions shown in Fig. 6 will occur at some station on the forebody, and the following scenario for the generation of wing rock can be envisioned.

Even a very small spin rate, resulting from the wing-body response to some disturbance, will determine the separation asymmetry, as is demonstrated by the measured[8] C_Y reversal at $p_N \approx 0$ in Fig. 9. Keener's flow visualization results[9] (Fig. 10) illustrate the finite extent of the critical-flow region. When the free-to-roll model in Fig. 1 responds to some disturbance, a rolling motion is initiated. The final turbulent crossflow separation is moved downstream on the right side in Fig. 7 through the generated upstream moving-wall effect on transition, as was discussed earlier, and on the opposite left side, the turbulent separation moves upstream. This separation asymmetry (with associated vortex asymmetry) will grow from half cycle to half cycle of the roll oscillation as the roll amplitude grows (see Fig. 1) and with it the corresponding moving-wall velocity U_W. Thus, the asymmetry-induced local-side force and the corresponding vortex-strength-asymmetry will grow with the increasing U_W/U_∞ ratio, as is illustrated by the $-C_\ell$ characteristics in Fig. 6 for $U_W/U_\infty < 0.2$.

In addition to this growth of the azimuthal extent of the separation asymmetry, there is also a growth of the axial extent. The flow separation will extend forward on the nose until it finds a cross section where a lower cross-flow Reynolds number compensates for the increased moving-wall effect, giving the combination of Re and U_W/U_∞ that creates the subcritical separation switch illustrated by the Magnus lift reversal in Fig. 4. Conversely, the other end of the flow-separation region moves downstream on the nose to a cross section where a higher cross-flow Reynolds number compensates for the increased moving-wall effect, producing the supercritical separation switch illustrated by the Magnus lift reversal in Fig. 5.

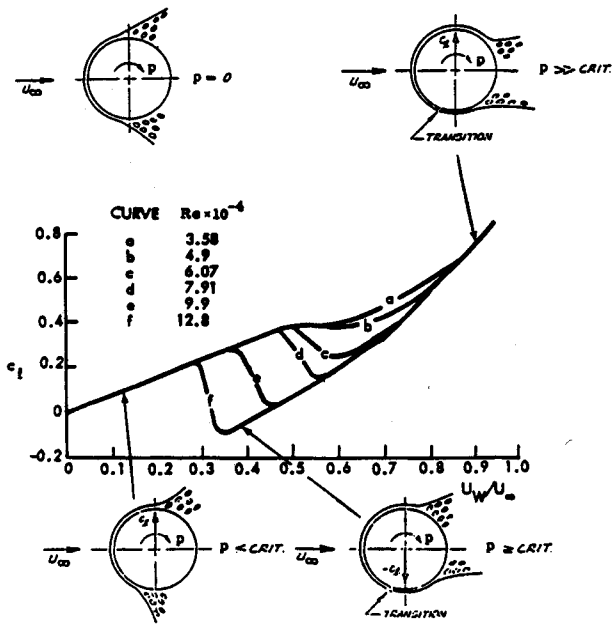

Fig. 4 Moving-wall effect on a rotating circular cylinder with laminar initial flow conditions (Ref. 5).

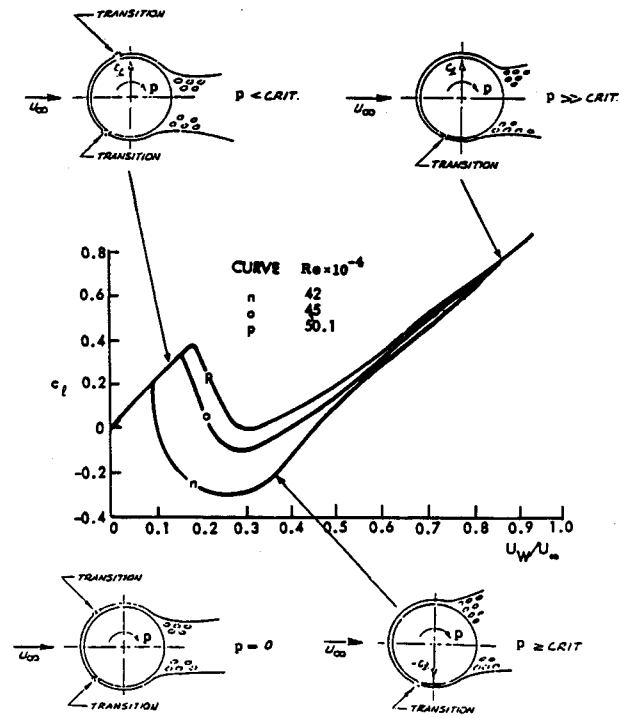

Fig. 5 Moving-wall effect on a rotating circular cylinder with turbulent initial flow conditions (Ref. 5).

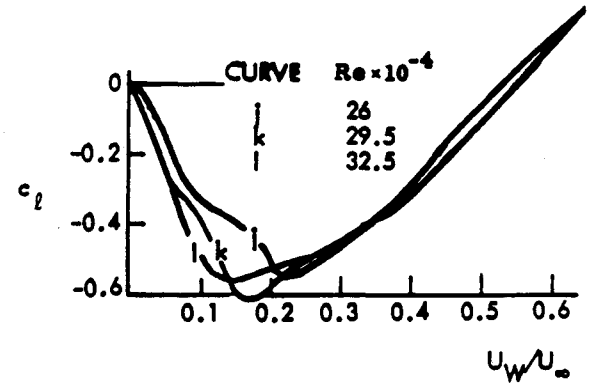

Fig. 6 Measured Magnus lift on a rotating circular cylinder at critical-flow conditions (Ref. 5).

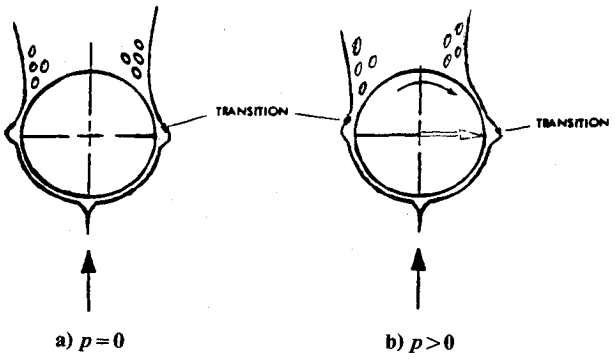

Fig. 7 Moving-wall effect on the laminar separation bubble on a rotating circular cylinder (Ref. 4).

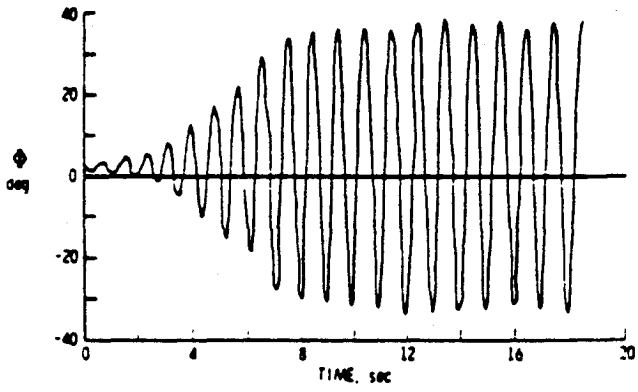

Fig. 8 Wing rock buildup at α = 27 deg for a sharp-edged 80-deg delta wing (Ref. 7).

Thus, when the flow separation is initially symmetric, and the asymmetry is generated completely by the coupling between crossflow transition and body spin, all three of the flow processes generating negative Magnus lift (see Figs. 4–6) contribute to the half-cycle to half-cycle growth of the vortex strength and with it the wing-rock amplitude. This explains the explosive amplitude growth (see Fig. 1) compared to that for a slender delta wing[7] (see Fig. 8). In the latter case, the vortex strength remains constant from half cycle to half cycle.

For initially asymmetric flow conditions, at $\alpha > 2\theta_A = 38$ deg (for the same configuration), the very powerful critical-flow mechanism is eliminated, explaining the cessation of the growth of the wing-rock amplitude when the angle of attack exceeds $\alpha = 38$ deg (see Fig. 3a). It is also the reason for the recurrence of the wing rock for the forward wing position at $\alpha \geq 40$ deg (see Fig. 3b). The asymmetric flow condition, existing initially on the nose, will provide asymmetric vortices that can generate the roll rate needed to produce the transition effects discussed in Ref. 2, which in turn produce the asymmetry-switching process that drives the wing rock of the axisymmetric body.[2] But, what is the reason for the recurrence of wing rock at low angles of attack, $\alpha < 30$ deg (see Fig. 3b)?

It has been shown[6] that the effective Reynolds number is well approximated by that for the wetted length between the stagnation point and the lateral azimuth in the crossflow plane A-A in Fig. 11, inclined an angle σ to the body axis. However, this holds true only if both $\alpha \geq 30$ deg, and the cross-sectional area is constant. In the present case of interest, both these conditions are violated, and transition occurs through a much faster (lower *Re*) three-dimensional process, as has been described for slender bodies of revolution at low angles of attack.[10] Even without considering the significant upwash from the wing in its forward location, symmetric flow

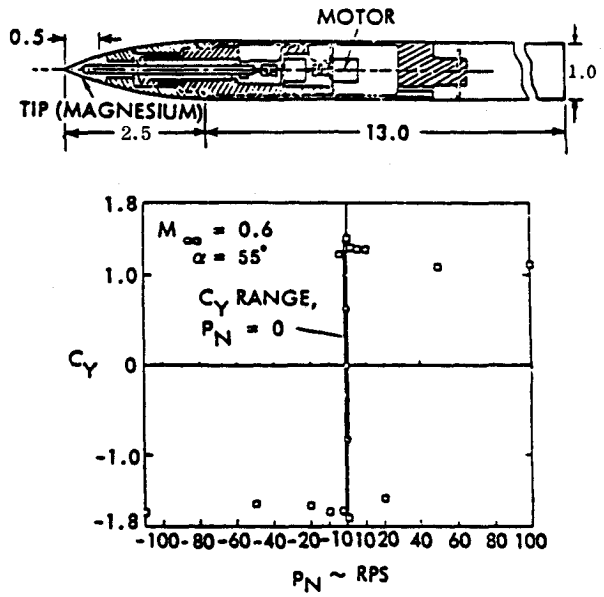

Fig. 9 Effect of a spinning-nose tip on the side force of an ogive-cylinder at α = 55 deg and M_∞ = 0.6 (Ref. 8).

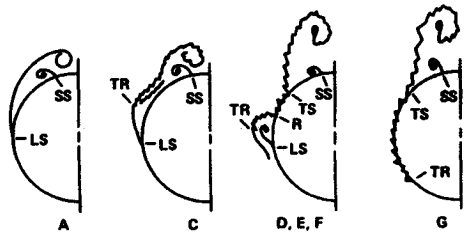

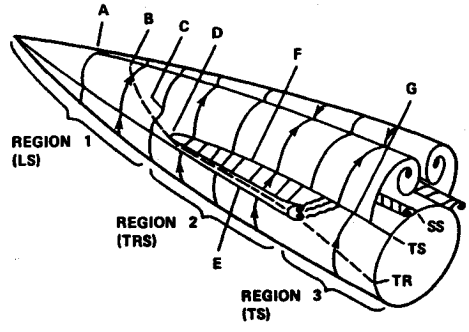

Fig. 10 Geometry of the critical flow region on a pointed 3.5 caliber ogive at α = 40 deg and M_∞ = 0.25 (Ref. 9).

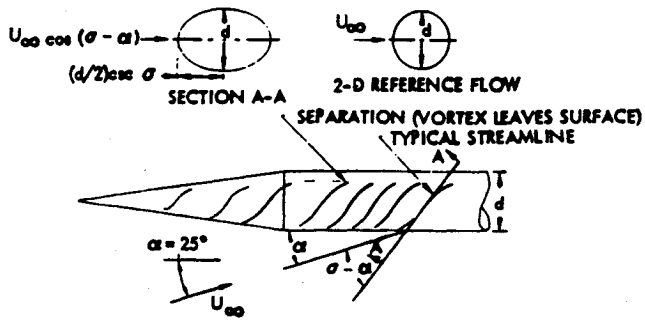

Fig. 11 Crossflow streamlines on a slender axisymmetric body at high angles of attack (Ref. 6).

separation with associated forebody vortices would occur at $\alpha > \theta_A = 19$ deg. Instead of the low-α situation[10] shown in Fig. 12a, one would have the one sketched in Fig. 12b for moderately high angles of attack, a flow geometry very similar to the one described in Ref. 2, to be causing the wing rock for the aft-wing position. Because of the wing-induced upwash, one can expect the forebody flow separation with associated body vortices to be present down to lower angles of attack than $\alpha = 19$ deg, which is in agreement with the data trend in Fig. 3b.

For the aft-wing position, the wing-induced upwash effect on the nose should be negligible. However, one would still expect symmetric forebody vortices to appear at $\alpha \geq 19$ deg. The "dip" in the wing-rock amplitude curve at $\alpha \approx 25$ deg (see Fig. 3a) may be tied to the "transition" between three-dimensional and two-dimensional transition mechanisms.

Effect of Cross-Sectional Shape

The roll angle has no effect on the symmetry of the vortex pair above a circular cross section. It does, however, affect the vortex geometry above the horizontal and vertical elliptical cross sections, as is illustrated by the flow sketches made from smoke flow visualization at $\alpha = 30$ deg[3] (see Fig. 13). The difference between the horizontal-elliptic and circular cross sections is that in the former case, ϕ and $\dot{\phi}$ effects together provide the vortex-induced restoring rolling moment through the downwash effect on the wing; whereas the $\dot{\phi}$ effect alone does it for the circular section. In both cases, however, the effect of body spin on transition is the same, i.e., to reverse the rolling moment. Consequently, the wing-rock characteristics for the two cross sections are largely similar (see Fig. 3). The earlier start of the wing rock buildup for the horizontal, elliptic cross section simply reflects the fact that, even without wing-induced upwash effects, symmetric vortices will start already at $\alpha = 15$ deg as the apex angle of the nose profile is $\theta_A = 15$ deg, not $\theta_A = 19$ deg, as in the case of the circular cross section.

For the forward wing position, the nose with vertical, elliptic cross section generates wing-rock characteristics that are completely different from those for the models with either a circular or a horizontal-elliptic forebody cross section (see Fig. 3b). Smoke flow streamlines[3] show the two body vortices to interact with each other in the manner described in Fig. 14. That is, the side wash from the lifted-off, upperbody vortex causes the low, active body vortex to move across the fuselage to induce suction lift on the opposite wing. It can be seen that this vortex-induced lift produces a restoring, statically stabilizing rolling moment, providing the aerodynamic spring needed for the wing-rock motion.[11] As was the case for the circular cross section,[2] the change of forebody vortex geometry, in this case caused by a roll deflection at apex through $\phi = 0$, takes a certain time Δt to be convected down to the wing.

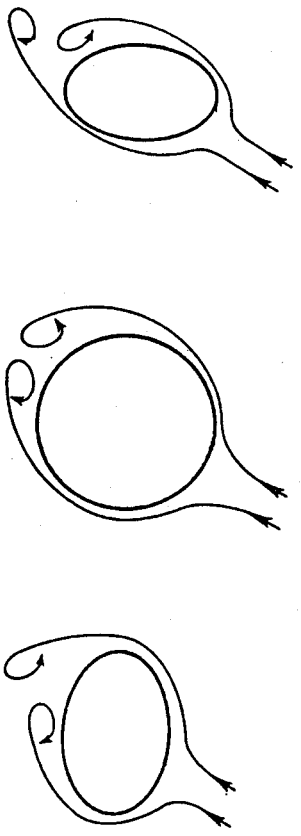

Fig. 13 Effect of cross-sectional shape on crossflow separation at $\alpha \geq 30$ deg (Ref. 3).

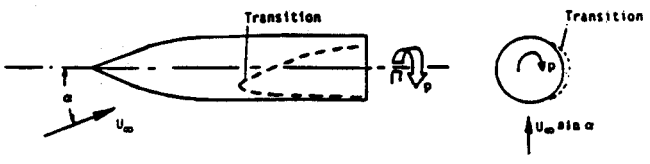

a) Low angles of attack (Ref. 10)

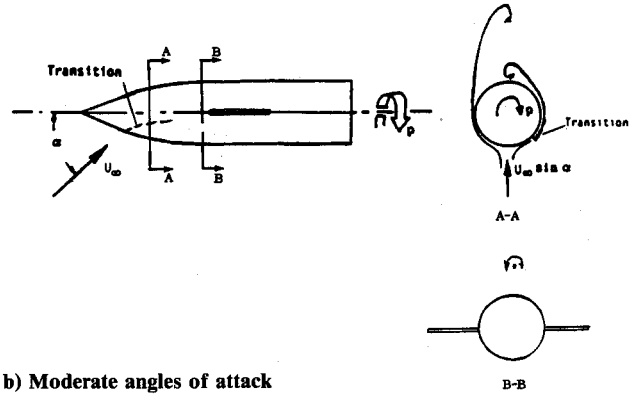

b) Moderate angles of attack

Fig. 12 Effect of body spin on transition.

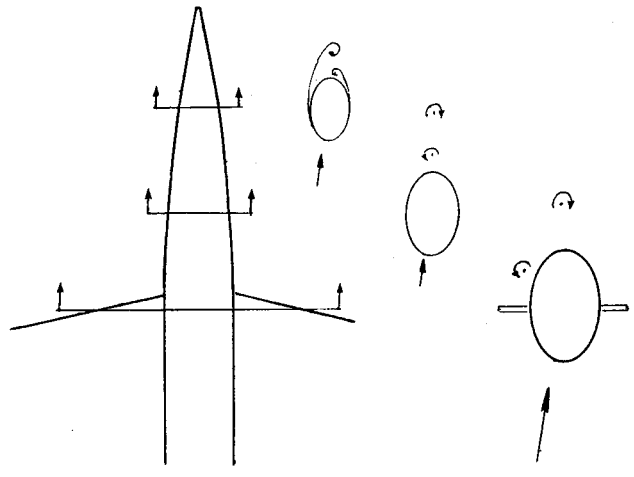

Fig. 14 Crossflow separation and vortex development for the vertical-elliptic cross-sectional forebody.

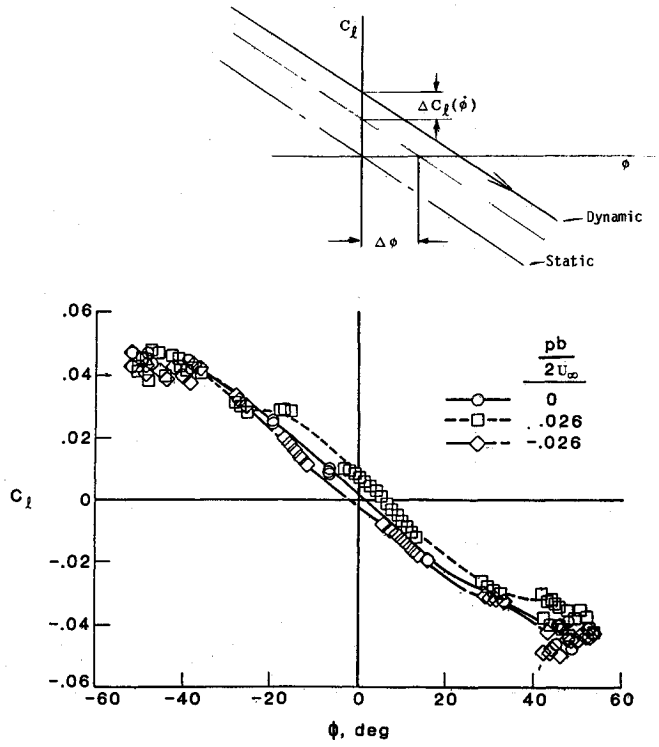

Fig. 15 Rolling moment coefficient during wing rock at α = 35 deg (Ref. 3).

This time lag causes the vortex-induced statically stabilizing rolling moment to be dynamically destabilizing, driving the wing-rock motion. This undamping action is clearly visible in the C_ℓ loop observed during wing rock[3] (see Fig. 15). The maximum offset between the upstroke or downstroke portions of the dynamic $C_\ell(\phi)$ loop and the static $C_\ell(\phi)$ characteristics, (which will occur at $\phi = 0$, where $\dot\phi$ is the maximum) would be $\Delta\phi = \dot\phi\Delta t$ due to the time lag effect. Note that the C_ℓ-offset at $\phi = 0$ is such that it will drive the rolling motion, i.e., the effect is undamping.

According to experimental results for a trisurface, biconic configuration, presented by Orlik-Rückemann in his review of high alpha aerodynamics,[12] the time lag for the forebody vortex is

$$\Delta t = x/\bar U \tag{1}$$

where x is the distance from apex and $\bar U = 0.8\ U_\infty$. Thus, $\Delta\phi$ becomes

$$\Delta\phi = \frac{\dot\phi x}{\bar U} = 2.5\,\frac{x}{b}\,\frac{pb}{2U_\infty} \tag{2}$$

For the laminar flow conditions of the test, reported in Ref. 12, the vortex asymmetry is generated at the apex, similarly to what is the case for the slender wing rock.[11] However, when spin-induced moving-wall effects on crossflow transition are involved, as in the present case, causing a separation asymmetry of the type shown by Keener[9] (see Fig. 10), the asymmetry starts aft of the apex. Thus, the distance from the apex to the wing trailing edge is the maximum distance that would be involved in the convective process. That is, for the forward wing position, $x/d < c_r d + l_N/d$. With $l_N/d = 4$, $c_r/d = 3.38$, and $b/d = 9.16$, one obtains $x/b < 0.81$, which in Eq. (2) gives $\Delta\phi < 3.0$ deg for $pb/2U_\infty = 0.026$. Even this very generous estimate of the time-lag effect cannot account for the observed maximum phase shift in Fig. 15 of $\Delta\phi \approx 5.5$ deg.

The difference between the estimated phase lag due to the time lag and the one measured in the test is caused by moving-wall effects. Including moving-wall effects for the flow sketch in Fig. 14 gives the flow picture sketched in Fig. 16. The downstream moving-wall effect will delay crossflow separation on the nose, causing the lower, active vortex to move farther toward the opposite wing, resulting in increased suction and an associated increase $\Delta C_\ell(\dot\phi)$ of the magnitude of the statically stabilizing vortex-induced rolling moment (see inset in Fig. 15). Thus, as in the case of dynamic stall,[13] the overshoot of the static characteristics has two components: one, $\Delta\phi = \dot\phi\Delta t$, due to time lag, and the other $\Delta C_\ell\ (\dot\phi)$, due to the dynamic force overshoot generated by the moving-wall effect.

In order for wing rock to result, which is a limit-cycle-type motion, the loop portions away from $\phi = 0$ in Fig. 15 must contribute roll damping. Such a "figure eight" trend is in-

Fig. 16 Conceptual moving-wall effect on forebody flow separation and vortex development.

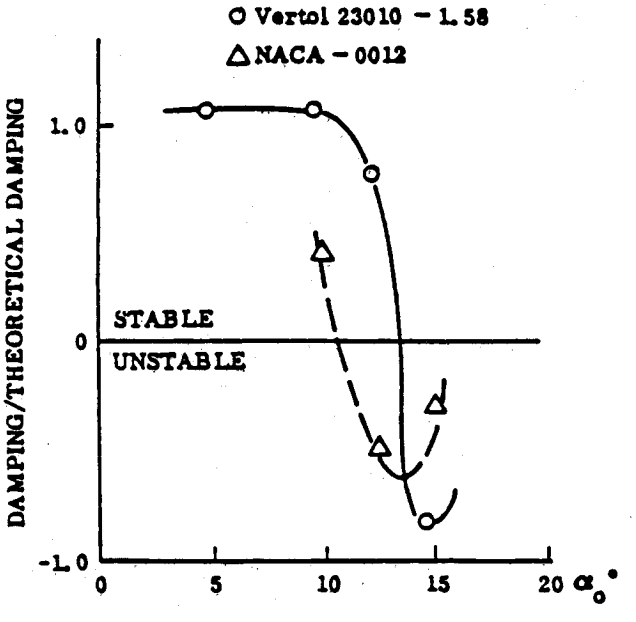

Fig. 17 Damping in plunge for an airfoil in the stall region (Ref. 14).

dicated for $\phi<0$ in Fig. 15. What can produce such a damping trend? Aerodynamic damping will be produced by the wing when the roll angle ϕ has reached values high enough to produce $\alpha_{\text{eff}} < \alpha_s$

$$\alpha_{\text{eff}} = \arctan(\alpha_o \cos\phi) \tag{3}$$

In that case, damping in plunge is experienced by the local airfoil section[14] (see Fig. 17), and positive roll damping will be produced. (Note that for the aspect ratio 4 wing in Fig. 2, the stall angle is moved to $\alpha_s \approx 20$ deg from $\alpha_s \approx 12$ deg in Fig. 17.) As the roll rate decreases towards the end of the roll deflection, the damping action (for the same damping coefficient) will be less than the undamping action of the forebody vortices around $\phi = 0$, where the roll rate reaches its maximum. That means that ϕ has to exceed greatly the value giving $\alpha_{\text{eff}} = \alpha_s$ in Eq. (3) before enough damping has been generated to balance the undamping, generated at lower ϕ by the forebody vortices. This is the reason for the explosive growth of the wing-rock amplitude for the forebody with the vertical elliptic cross section (Fig. 3b).

For the aft wing position, the lower forebody vortex will be higher above the wing than what is shown in Figs. 14 and 16, resulting in a decreased suction force compared to that for the forward wing position. This explains the lesser wing rock amplitude at $\alpha < 40$ deg (compare Figs. 3a and 3b).

Going back to Fig. 15, it is difficult to distinguish any damping loops at large ϕ values, except for the data trend showing a crossover at $\phi \approx 20$ deg. Figure 17 shows a possible reason for the lack of distinctive data trends. Before the final damping action is experienced at $\alpha_{\text{eff}} < \alpha_s$, negative damping will occur when α_{eff} is close to the static stall angle α_s. Another problem with the data resolution in Fig. 15 is that the rolling moment coefficient was not measured directly but was estimated based upon the free-to-roll motion data.[3]

Conclusions

A detailed analysis of the experimentally observed wing rock of a generic aircraft configuration has led to the following conclusions.

1) Wing rock generated by forebody vortices will in general be more severe than the slender wing rock generated by leading-edge vortices.

2) Small changes of the aircraft geometry can cause different flow mechanisms to be the dominant ones generating the wing rock.

The general observation is that wing rock generated by forebody vortices is the type of wing rock to which most current and future advanced aircraft will be exposed.

Acknowledgments

The results presented in this paper were in part developed under contract to Fluid Dynamics Lab/FIGC, Wright Patterson Air Force Base, Contract F33615-87-C-3607, monitored by W. B. Blake.

References

[1]Brandon, J. M. and Nguyen, L. T., "Experimental Study of Effects of Forebody Geometry on High Angle of Attack Stability," *Journal of Aircraft,* Vol. 25, July 1988, pp. 591–597.

[2]Ericsson, L. E., "Wing Rock Generated by Forebody Vortices," *Journal of Aircraft,* Vol. 26, Feb. 1989, pp. 110–116.

[3]Brandon, J. M., Murri, D. G., and Nguyen. L. T., "Experimental Study of Effects of Forebody Geometry on High Angle of Attack Static and Dynamic Stability and Control," International Council of Aeronautical Sciences, ICAS Paper 86-5.4.1, Sept. 1986.

[4]Ericsson, L. E., "Moving Wall Effects in Unsteady Flow," *Journal of Aircraft,* Vol. 25, Nov. 1988, pp. 977–990.

[5]Swanson, W. M., "The Magnus Effect: A Summary of Investigations To Date," *Journal of Basic Engineering,* Vol. 83, Sept. 1961, pp. 461–470.

[6]Ericsson, L. E. and Reding, J. P., "Asymmetric Vortex Shedding from Bodies of Revolution," *Progress in Astronautics and Aeronautics: Tactical Missile Aerodynamics,* Vol. 104, edited by M. J. Hemsch and J. N. Nielsen, AIAA, New York, 1986, pp. 243–296.

[7]Nguyen, L., Yip, L., and Chambers, J., "Self-Induced Wing Rock of Slender Delta Wings," AIAA Paper 81-1883, Aug. 1981.

[8]Fidler, J. E., "Active Control of Asymmetric Vortex Effects," *Journal of Aircraft,* Vol. 18, April 1981, pp. 267–272.

[9]Keener, E. R., "Flow-Separation Patterns on Symmetric Forebodies," NASA TM-86016, Jan. 1986.

[10]Ericsson L. E., "Coupling Between Vehicle Motion and Slender Cone Transition," *AIAA Journal,* Vol. 25, Sept. 1987, pp. 1194–1198.

[11]Ericsson, L. E., "The Fluid Mechanics of Slender Wing Rock," *Journal of Aircraft,* Vol. 21, May 1984, pp. 322–328.

[12]Orlik-Rückemann, K. J., "Aerodynamic Aspects of Aircraft Dynamics at High Angles of Attack," *Journal of Aircraft,* Vol. 20, Sept. 1983, pp. 737–752.

[13]Ericsson, L. E. and Reding, J. P., "Fluid Mechanics of Dynamic Stall, Part I., Unsteady Flow Concepts," *Journal of Fluids and Structures,* Vol. 2, Jan. 1988, pp. 1–33.

[14]Liiva, J., Davenport, F. J., Gray, L., and Walton, I. C., "Two-Dimensional Tests of Airfoils Oscillating Near Stall," U.S. Army Aviation Materials Labs., Fort Eustis, Virginia, TR 68-13 A and B, April 1968.